Self-Enhancement of Efficiency and Self-Attenuation of Hysteretic Behavior of Perovskite Solar Cells with Aging

Yuxi Zhang,[a#] *Yanqing Zhu,*[a#] *Min Hu,*[c] *Narendra Pai,*[b] *Tianshi Qin,*[d] *Yi-Bing Cheng,*[e] *Udo Bach,*[b] *Alexandr N. Simonov,*[*f] *Jianfeng Lu**[a,b]

[a] *State Key Laboratory of Silicate Materials for Architectures, Wuhan University of Technology, 430070 Wuhan, P. R. China*

[b] *Department of Chemical Engineering, ARC Centre of Excellence for Exciton Science, Monash University, Victoria 3800, Australia*

[c] *School of Electronic and Electrical Engineering, Hubei Province Engineering Research Center for Intelligent Micro-Nano Medical Equipment and Key Technologies, Wuhan Textile University, Wuhan 430200, P. R. China*

[d] *Key Laboratory of Flexible Electronics (KLOFE) & Institute of Advanced Materials (IAM), Jiangsu National Synergistic Innovation Center for Advanced Materials (SICAM), Nanjing Tech University, 30 South Puzhu Road, Nanjing 211816, P. R. China*

[e] *State Key Laboratory of Advanced Technology for Materials Synthesis and Processing, Wuhan University of Technology, Wuhan 430070, P. R. China*

[f] *School of Chemistry, Monash University, Victoria 3800, Australia*

[#] *These authors contributed equally.*

Abstract

Spontaneous enhancement of the photovoltaic performance of perovskite solar cells (PSCs) after aging has been reported, but the underlying reasons for such behavior are still under debate. Herein, we demonstrate that this spontaneous improvement effect accompanied by self-attenuation of hysteresis in the current–voltage characteristics is time- and temperature-dependent. Moreover, it is universal to PSCs based on a range of mixed-ion perovskites, and coupled to different hole and electron transporting materials. Time-resolved confocal fluorescence microscopy and other characterization techniques suggest that the "self-healing" phenomenon is accompanied by the homogenization and enhancement in the charge extraction efficiency as well as suppressed recombination throughout cm^2-scale perovskite layers. These dynamic effects need to be accounted for when assessing the initial and stabilized performance of PSCs.

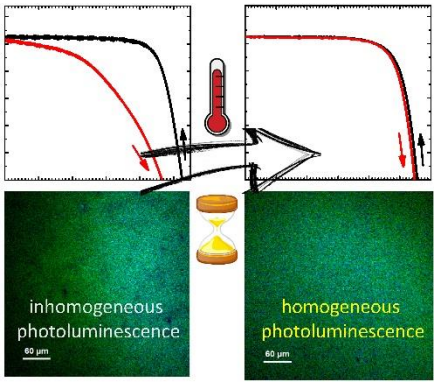

Over the recent years, metal-halide perovskites have become one of the most intensively investigated class of materials.[1] Power conversion efficiency (PCE) above 25 % of the perovskite solar cells (PSCs) are now feasible with optimized mixed ion perovskite compositions and processing.[2-3] Notwithstanding remarkably rapid improvements in the performance, many fundamental principles underpinning the evolution of the PSCs in operation and during storage are yet to be understood. One actively investigated aspect relevant to the majority of PSCs is the nature of the processes giving rise to the scan-dependent hysteresis in the current (*J*) – voltage (*V*) curves, which is often found even with the devices having efficiency over 25%.[2, 4-5] The recently reported 'inverted hysteresis' phenomenon even further complicates the problem.[6-7] This behavior creates ambiguity in respect to the working mechanism of the solar cells and remains one core challenge on our pathway to achieving stable and reliable performance of the perovskite photovoltaics.[8]

Many fundamental studies on the PSC hysteresis have been reported.[9-11] A large body of evidence suggests that the physicochemical origin of the hysteretic behavior of PSCs is the migration of mobile ionic species, most likely halide ions and their vacancies, within the perovskite layer and ensuing field screening effects.[12] Efforts have been made to suppress the hysteresis by optimization of the precursor composition,[13] interfaces,[14] quality of the perovskite film,[3] as well as passivation of defects,[15] achieving solar cells with high efficiency and negligible hysteresis. Many initial studies on these effects analyzed the *J-V* data for as-prepared and/or aged devices in terms of the so-called "hysteresis index" *H*-index = $(PCE_{Rev} - PCE_{Fwd})/PCE_{Rev}$, where PCE_{Rev} and PCE_{Fwd} are PCEs derived from the reverse (forward bias to short circuit, FB to SC) and forward (short circuit to forward bias, SC to FB) scans, respectively.[16-18] However, more recent investigations showed that the hysteresis as well as the *J-V* efficiency of PSCs are dynamic rather than static parameters.[19-22] For example, several research groups have reported that solar cells based on mixed-perovskites, including Pb^{2+} or

Sn^{2+} based perovskites, reach their highest PCE values and minimum hysteresis after a few days of ambient storage in the dark.[18, 23-26]

Several research groups suggested that change in the trap density within the perovskite film might be a major factor driving the spontaneous improvement of the PCE of PSCs during storage.[24-29] Mechanisms proposed to explain this self-enhancement include passivation by sodium ions liberated from the glass substrate into the $MAPbI_3$ perovskite layer (MA^+ – methylammonium),[28] self-de-doping of perovskite or recrystallization of $MAPbI_3$-based perovskite film,[24, 26] coalescence of the $Cs_{0.05}FA_{0.79}MA_{0.16}PbI_{2.49}Br_{0.51}$ (FA^+ – formamidinium) crystals.[18] Moghadamzadeh *et al.* disputed the hypothesis of change in the grain and crystallite sizes as they did not find any evidence for such change in the $Cs_x(FA_{0.83}MA_{0.17})_{(1-x)}PbI_{2.49}Br_{0.51}$ (x = 0, to 0.05, 0.1, 0.15) perovskite crystallites.[25] Instead, they observed the reduction in trap-assisted non-radiative recombination, which was ascribed to strain relaxation of the perovskite lattice. Cho *et al.* reported that spontaneous PCE improvement results from the change in the charge recombination mechanism from surface- to bulk-dominated due to the defect passivation at the perovskite surface upon storage, as well as from the improved conductivity and energy alignment of the hole transporting material (HTM).[23]

Notwithstanding active research in the field, studies on the evolution of the PCE and hysteretic behaviour of PSCs during the initial storage are rare and are sometimes contradictory, as summarised above and also in Table S1. Aiming to further the udnerstanding of these important phenomena, the present work investigates evolution of the properties of solar cells based on single and mixed-cation perovskite compositions and different selective-charge transfer materials, rather than focusing on a single PSC configuration. Another important feature of this study is the analysis of the kinetics of the investigated processes as a function of temperature. By coupling the analysis of the *J-V* behavior under various conditions to the device morphology, transient photovoltage/photocurrent decay, and time-resolved confocal

fluorescence microscopic studies, we question the significance of the interface reactions and/or charge transport materials to the self-improvement phenomenon while demonstrating that aging results in the homogenisation and enhancement of the charge-transfer as well as supressed recombination within the perovskite layer.

Unless specified otherwise, solar cells investigated in this work had a typical *n–i–p* (FTO|*c*-TiO_2|*m*-TiO_2+perovskite|HTM|Au) architecture (Figure 1a; FTO – fluorine-doped tin(IV) oxide, *c*-TiO_2 and *m*-TiO_2 – compact and mesoporous titania, respectively), and were fabricated by sequential deposition of components onto glass covered with fluorine-doped tin(IV) oxide, which served as a cathode in the final device. Optimized PSC fabrication procedures adopted from the literature and established in our laboratories were employed.[3, 14] The active surface area of the devices was 1.00 cm^2. The examined solar cells featured a *ca.* 150 nm mesoporous titania scaffold (30 nm particle size) impregnated with perovskite absorber. The perovskite film thickness was reported to affect the hysteresis in PSCs, though the existing evidence is controversial. While Correa-Baena *et al.* reported a decrease in the hysteresis with an increase in the active layer thickness (supported on *c*-TiO_2|*m*-TiO_2 ETM),[30] Cho *et al.* demonstrated an opposite trend (using *c*-TiO_2 ETM).[31] To avoid any additional ambiguities, all perovskite films examined herein had the same thickness of 350-400 nm.

In our experiments (see Supporting Information for details), all freshly prepared solar cells exhibited a pronounced hysteresis during *J-V* measurements (scan rate 0.100 V s^{-1}) with *H*-index ranging from 0.2 to 0.5. As shown in Figure 1b, the overall performance spontaneously and continuously improved and hysteresis diminished while keeping the encapsulated devices in the dark. For example, when stored at room temperature 22 °C, the PCE_{Rev} of a typical $Cs_{0.05}FA_{0.79}MA_{0.16}PbI_{2.49}Br_{0.51}$ perovskite solar cell increased from 16.4 ± 0.3% to 17.9 ± 0.9%, while PCE_{Fwd} enhanced from a low value of 9 ± 2 % to 15.1 ± 1.3 % over initial 313 h. These efficiencies are comparable to those reported previously for encapsulated devices with 1 cm^2

active area.[32-34] After 1113 h, the PCE_{Rev} slightly decreased to 16.6 ± 1.4% and the PCE_{Fwd} increased to 16 ± 2 %. As a result of these changes, the hysteresis gradually decreased over the duration of the experiments and equilibrated at a close to zero level after approximately 600 h.

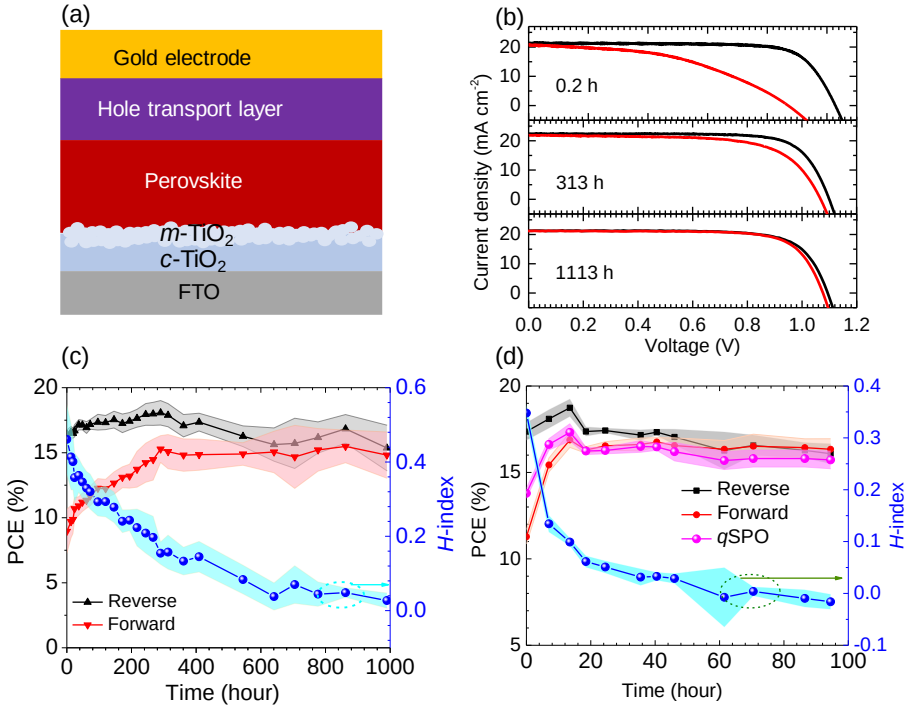

Figure 1. (a) The device architecture scheme of the solar cells examined in this study; (b) reverse (*black*) and forward (*red*) *J-V* curves (scan rate 0.100 V s^{-1}) for devices recorded after storage in the dark at 22 °C for 0.2, 313 and 1113 h; (c) PCE derived from the reverse (*black*) and forward (*red*) *J-V* scans, and *H*-index (*blue*) of the devices aged in the dark at 22 °C; (d) PCE derived from the reverse (*black*) and forward (*red*) *J-V* scans, quasi-stabilized power output after 60 s (*q*SPO, *magenta*) and *H*-index (*blue*) of the devices aged in the dark at 45 °C. The perovskite composition was $Cs_{0.05}FA_{0.79}MA_{0.16}PbI_{2.49}Br_{0.51}$ and the HTM was doped spiro-OMeTAD. In panels (c-d), symbols and colored areas show average values and standard deviations for 5 independent devices of each type, respectively.

The major improvement in *H*-index from 0.46 ± 0.09 to 0.16 ± 0.04 occurred over the initial 313 hours, followed by a slower self-attenuation down to 0.03 ± 0.02 after 1113 hours (Figure 1c). Importantly, the quasi-stabilized power output (*q*SPO) derived by holding the cells at a fixed voltage near the maximum power point for 60 s also changed during storage, showing a similar trend found for PCE_{Fwd} with the initial enhancement and subsequent stabilization in the performance (Figure 1d and Figure S1). In these experiments, the average *q*SPO values

were slightly lower than the PCE_{Fwd} and PCE_{Rev} after 20 h storage. According to Miyasaka *et al.*,[35] this might be associated with the movement of ions or vacancies from the perovskite bulk to the interfaces/contacts under continuous light-soaking, which slows down the carrier extraction. Hoke *et al.* also observed similar phenomenon and attributed it to the emergence of photo-induced trap states during continuous operation.[36]

We also found that the spontaneous enhancement might be a general phenomenon for the mixed cation perovskite based devices (Figure S2 and Table S1). This conclusion was made from the tests of PSCs based on the double cation perovskite $FA_{0.83}MA_{0.17}PbI_3$ with a single anion and $FA_{0.85}MA_{0.15}PbI_{2.55}Br_{0.45}$ with mixed anions, which also exhibited a self-improvement behavior similar to that described above for the triple-cation double-anion $Cs_{0.05}FA_{0.79}MA_{0.16}PbI_{2.49}Br_{0.51}$ perovskite (Figures S2 and S3, Table S1). At the same time, the classical single-cation perovskite $MAPbI_3$ did not demonstrate a significant decrease in *H*-index and notable enhancements in the PCE (Figure S4 and Table S1). These observations suggest that the dynamics of hysteresis and efficiency evolution are in the first place dependent on the cationic composition of the perovskite.[37-39]

One possible explanation of the self-enhancement of the efficiency and self-attenuation of the hysteretic behavior is that the residual trapped solvents, *i.e.* DMF or DMSO within the perovskite layer, keep escaping during the aging, leaving a purer perovskite film with less defects. Indeed, it was reported that even heating at 150 °C for 15 min does not completely remove DMSO from the perovskite films due to its strong attachment to PbI_2.[40-41] To test this hypothesis, devices based on perovskite layers that were annealed at 100 °C for extended periods of time prior to the deposition of the hole-conducting material (HTM) were fabricated. However, this additional treatment did not induce any significant changes in their behavior during storage (Figure S5-S9). This observation indicates that any possible evaporation of solvent or other volatile components from the perovskite films does not contribute significantly

to the improvement in the performance with aging.

To further verify that the efficiency self-enhancement and hysteresis self-attenuation are associated with the processes within the perovskite layer, PSCs with different HTMs and electron transporting materials (ETMs) were tested. The $Cs_{0.05}FA_{0.79}MA_{0.16}PbI_{2.49}Br_{0.51}$ solar cells based on 2,2′,7,7′-tetrakis[N,N-di(4-methoxyphenyl)amino]-9,9′-spirobifluorene (spiro-OMeTAD),[8] poly[bis(4-phenyl)(2,4,6-trimethylphenyl)amine] (PTAA)[42] and 2,2′,7,7′-tetrakis(N,N′-di-p-methoxyphenylamine)-N,N′-bicarbazole (2,7-BCz-OMeTAD)[43] exhibit qualitatively similar behavior, though the kinetics of the processes responsible for the performance stabilization and *H*-index decrease depend on the chemical nature of HTM (Figure 2a, Figures S1, S10 and S11).[44] Considering that the preparation of the PTAA layer does not involve any oxidation reaction and that 2,7-BCz-OMeTAD is deposited as an additive-free material, negligible contributions of the effects associated with doping degree of HTM, or transformations/loss of *tert*-butyl pyridine (*t*BP) or lithium bis(trifluoromethanesulfonyl)imide (LiTFSI) additives in the hole-transporting layer is expected. Moreover, we have also demonstrated that devices based on spiro-OMeTAD with different levels of *p*-doping provided by the use of different cobalt complexes[33] exhibit identical, within error, behavior during storage (Figure S12). Tests of the devices with different ETMs produced similar conclusions. Indeed, PSCs based on SnO_2 as an electron transporting material demonstrated spontaneous improvement in performance during aging (Figure S13) similar to the devices with the TiO_2 ETM, which is consistent with previous reports.[25-26] These results suggest that changes in the perovskite rather than charge transporting layers are the major cause of the observed PSC self-healing phenomenon.

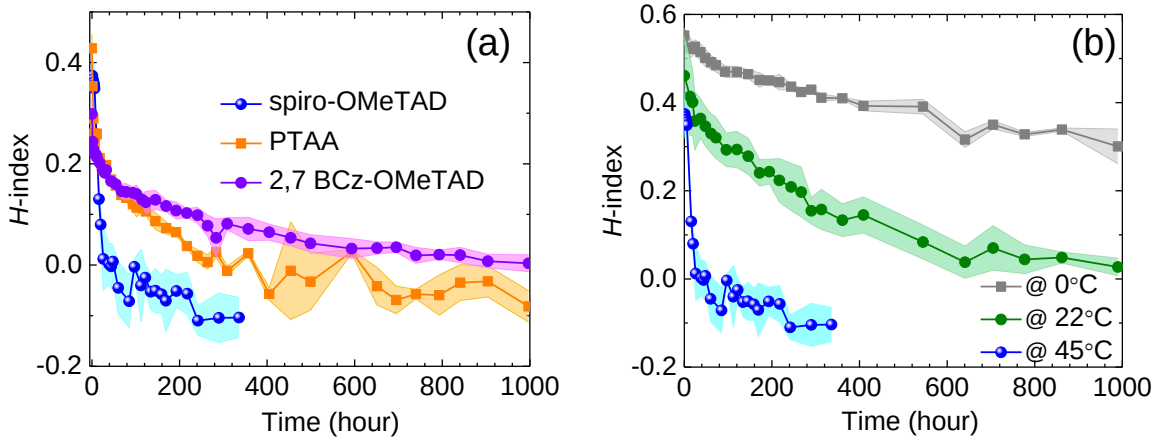

Figure 2. (a) Comparison of the *H*-index for PSCs based on spiro-OMeTAD (*blue*), PTAA (*orange*) and 2,7-BCz-OMeTAD (*purple*) HTMs aged in the dark at 45 °C; (b) evolution of *H*-index of the devices based on spiro-OMeTAD aged in the dark at 0 (*grey*), 22 (*green*) and 45 °C (*blue*). The device structure was FTO|c-TiO_2|m-TiO_2+$Cs_{0.05}FA_{0.79}MA_{0.16}PbI_{2.49}Br_{0.51}$|HTM|Au. Symbols and colored areas show average values and standard deviations for 5 independent devices of each type, respectively.

Notably, it was also found that the aging temperature affects the dynamics of the observed changes significantly, as concluded from the tests with the spiro-OMeTAD-based devices at 0, 22 and 45 °C (Figure 2b). During the low-temperature measurements, the degree of device self-attenuation was significantly reduced compared to the 22 °C measurements, and stabilization was not achieved even after 1000 h at 0 °C (Figure S14). As discussed above, the stabilization time was *ca* 600 hours at 22 °C (Figure S15), and decreased to as low as *ca* 24 hours at 45 °C (Figure S1). One process in perovskite materials that demonstrates pronounced dependence on temperature is the migration of ionic species or traps.[45-46] Hence, the results of experiments with mixed ion perovskites (Figures S2-S4) and different temperatures (Figure 2b, Figures S6, and S14-S15) collectively suggest that the self-attenuation behavior of PSC might be associated with changes in the perovskite composition throughout the layer supported by ion redistribution during aging. We have also estimated the apparent activation energy (E_a) of the investigated processes using the *H*-index transients obtained at different temperatures (Figure 2b) to be within the 10^1-10^2 kJ mol^{-1} range (Figure S16), which

compares well to the values reported for the migration of cations and halide ions in different perovskite materials.[47-48] However, we cautionary note the very high level of uncertainty in the E_a value reported herein.

Further, transient photovoltage and photocurrent decay (TPV and TPC) experiments[49] were undertaken to investigate the evolution of the charge transfer properties within solar cells while aging at 45 °C. Over 90 h of treatment, the charge recombination lifetime derived from the TPV data remained constant (Figure 3a), which indicates that the alteration of the interface charge recombination reaction within the devices is not the major reason for the observed significant self-improvement in the performance.[50] Analysis of the TPC data, which provides information on the competition between carrier sweep-out by the internal field and recombination within a working solar cell, indicates improved charge extraction after the initial 24 h of aging, which correlates with the decrease in the *H*-index and increase in the PCE. However, further changes in the TPC did not show a clear trend, which urged us to investigate the charge extraction processes in more detail using fluorescence lifetime imaging microscopy (FLIM) (*vide infra*).

X-ray diffraction patterns of as-prepared perovskite and of active layers of PSCs aged at 0, 22 and 45 °C for 24 h were also very similar (Figure 3b). Even though the mean crystallite size (*d*) calculated for the (110) peaks showed a small apparent increase after aging, the *d* values were the same within error for the samples conditioned at different temperatures. Thus, perovskite crystal size enlargement is unlikely to be responsible for the self-improvement behavior, which accords with the results of Moghadamzadeh *et al*.[25] Comparison of the top-view scanning electron micrographs of the freshly prepared perovskite layer with those of the perovskite layers kept for 24 h at 0 and 45 °C within fully-assembled devices did not reveal any noteworthy changes in the morphology and grain size upon aging either (Figure 3c-e, Figure S17). Similar observations were made using side-view imaging (Figure 3f-h). Thus, the

observed significant changes in the photovoltaic performance during storage can be hardly explained by structural and/or morphological changes.

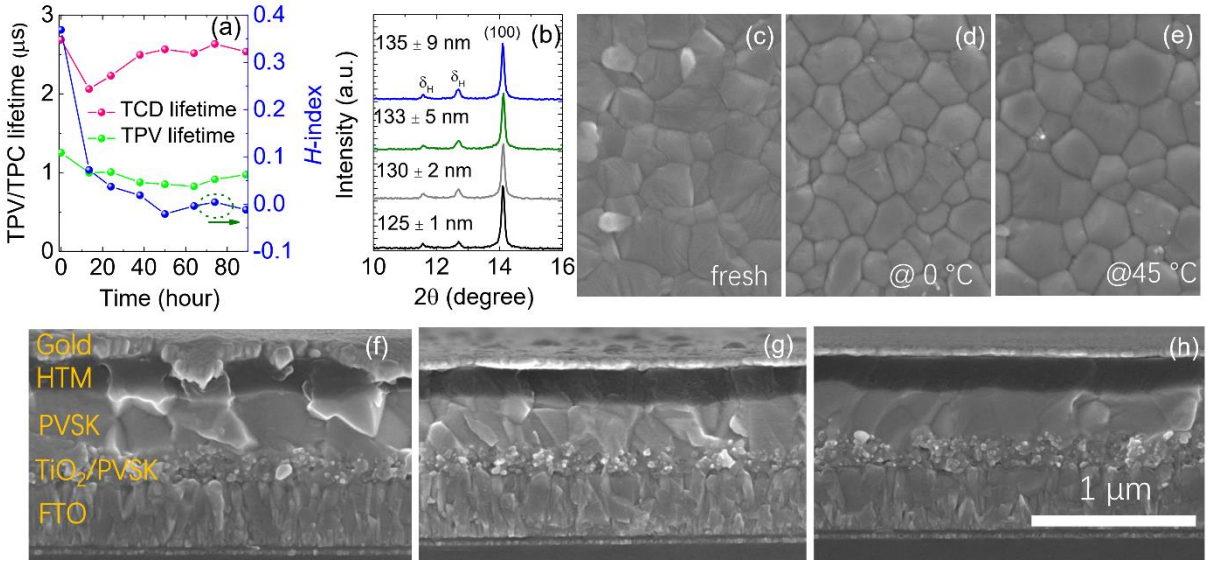

Figure 3. (a) Evolution of transient photovoltage (*pink*) and photocurrent (*light green*) lifetimes measured for encapsulated solar cells aged at 45 °C; corresponding *H*-index evolution data (*blue*) are shown for comparisons. (b) X-ray diffraction patterns for fresh $Cs_{0.05}FA_{0.79}MA_{0.16}PbI_{2.49}Br_{0.51}$ (*black*) and the perovskite layers aged for 24 h at 0 (*grey*), 22 (*red*), and 45 °C (*blue*) within fully assembled cells (spiro-OMeTAD and Au layers were removed by chlorobenzene prior to analysis); numbers show mean crystallite size (d_{XRD}) calculated for the (110) peak as mean values and standard deviation for three independent samples of each type. (c-h) Scanning electron microscopic analysis: top-view images of (c) freshly deposited $Cs_{0.05}FA_{0.79}MA_{0.16}PbI_{2.49}Br_{0.51}$ (2 h in the dark at 22 °C before analysis), and perovskite aged for 24 h at (d) 0, and (e) 45 °C within fully assembled cells (spiro-OMeTAD and Au layers were removed by chlorobenzene prior to analysis); side-view images of (f) as-fabricated device (*ca* 2 h in the dark at 22 °C before analysis), and similar PSCs aged for 24 h at (g) 0, and (h) 45 °C.

Finally, fluorescence lifetime imaging microscopy (FLIM) was applied for spatially-resolved quantitative analysis of the recombination and charge transfer properties of perovskite layers[51-54] before and after aging for 24 h at 45 °C within fully assembled cells (Figure 4). Similar to the SEM and XRD results discussed above, the "fresh" perovskite film samples in these experiments were also derived from the fully assembled cells by removing the HTM and Au immediately after deposition to avoid any effects of these deposition procedures on the active layer properties.

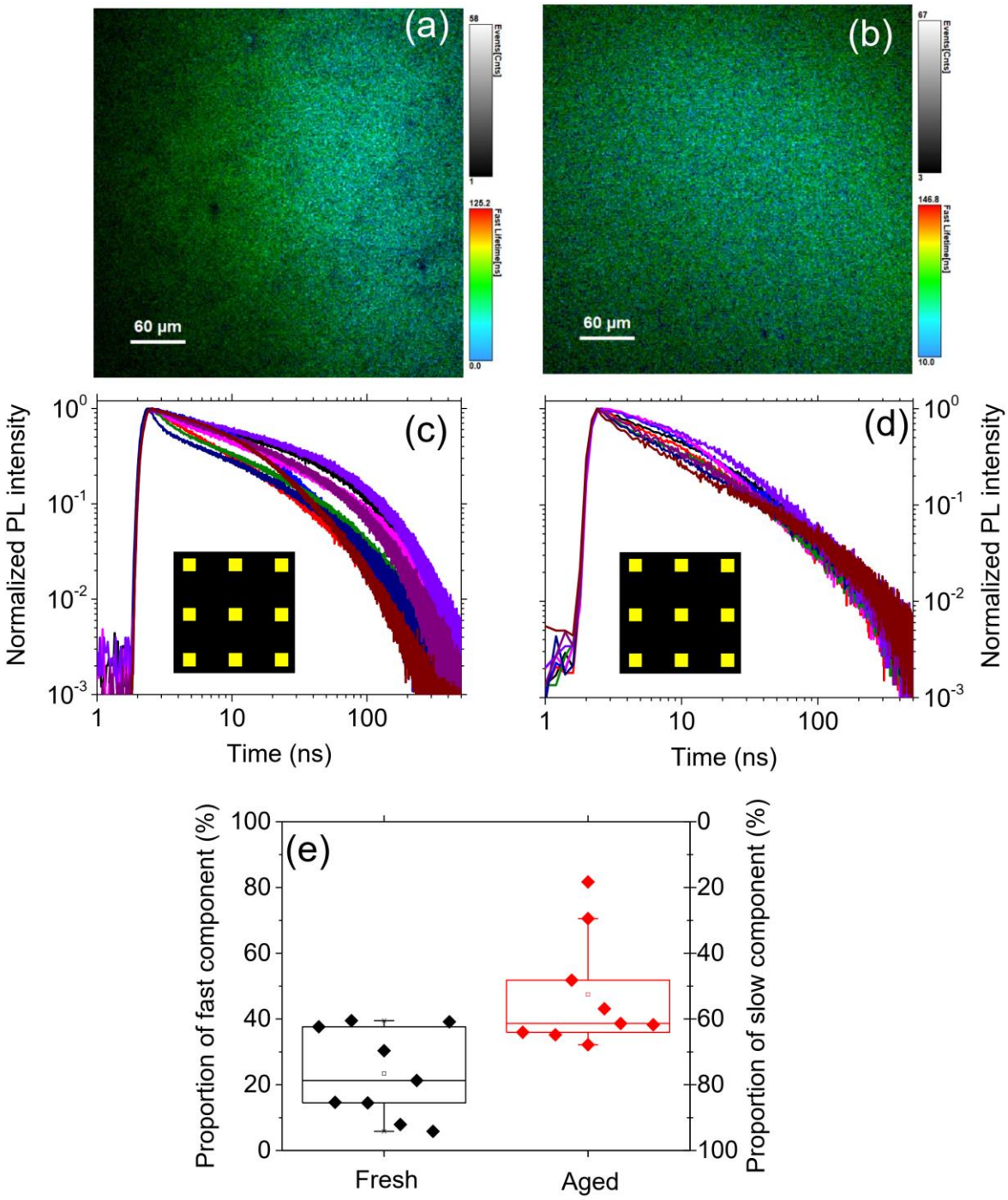

Figure 4. (a, b) Confocal PL lifetime maps, (c, d) time-resolved PL decay profiles, and (e) relative contributions of the fast (charge-extraction) and slow (recombination) components to the PL decay profiles for perovskite layers aged for 24 h at 45 °C within fully assembled cells (spiro-OMeTAD and Au layers were removed by chlorobenzene prior to analysis). Photoluminescence data were acquired with pulsed (confocal, 2 MHz repetition rate, 1 µJ cm^{-2} per pulse) 440 nm lasers. Yellow squares in panels c and d show the locations of the nine spots on the surface of the perovskite layer used for the analysis.

The sample after dark storage at 45 °C exhibited pronouncedly more uniform PL lifetime distribution within the layer as compared to the fresh film (Figure 4a-b). These results were further corroborated by the time-resolved PL (TRPL) data collected at nine different small spots located at the center and corners of the perovskite layer (Figure 4c-d). By fitting these experimental TRPL profiles with bi-exponential function, the average lifetimes of the device after aging were very close to each other (considering all experimental and fitting errors), ranging within *ca* 15-40 ns range. Contrasting this was the significant scatter of the values measured for different areas of the perovskite in the fresh device, which varied from *ca* 25 to 75 ns. The fitting parameters, *i.e.* lifetime and the corresponding amplitudes are listed in Table S2.

According to the literature,[55-56] slow and fast decay processes in the PL decay functions as those presented in Figure 4c-d are associated with the radiative recombination of free charge carriers due to traps in the bulk (higher τ_1) and change transfer at the ETM|perovskite interface (lower τ_2), respectively. Comparisons of the A_1 and A_2 parameters of the exponential fit functions (Table S3) suggests that the contribution of the productive charge carrier extraction process (A_2 and τ_2) to the recorded PL decay dependencies is enhanced after aging in the dark as compared to recombination (A_1 and τ_1) (Figure 4e).

The observed homogenization of the PL lifetimes within almost 2 cm^2 samples can be most plausibly interpreted in terms of improvement in the uniformity of the properties of the perovskite layer, which correlates with the enhancement in the power conversion efficiency and attenuation of the hysteresis of the PSCs. These improvements are highly unlikely to be supported by the interfacial processes, changes in the perovskite grain/crystallite size or within the ETM/HTM layers, as demonstrated through extensive control experiments described above. Thus, the most plausible explanation of the observed self-enhancement phenomenon is the progressive homogenization of the composition of the perovskite layer during storage in the

dark driven by the initially present concentration gradients. This hypothesis is supported by the temperature-dependent data presented herein (Figures 2b and S16). While halide migration within perovskites is well established,[57] migration and rotation of cations, such as FA^+, might be less facile though still possible.[47, 58-60] On the other hand, it was also reported that the large size of the FA^+ causes cage distortions, [PbI_6] octahedra tilting,[61] and local lattice strain[62] of the perovskite structure. During the storage, the lattice strain within the mixed-cation perovskites might relax and redistribute throughout the film, resulting in the observed improvements in the charge-transfer, suppressed recombination, attenuated hysteresis and higher PCE.

In summary, the present work demonstrates the universal ability of the perovskite solar cells based on multi-cation active materials to spontaneously improve their power conversion efficiency upon simple storage in the dark, irrespective of the chemical nature of the hole-transporting material. Collective evidence including the device performance tracking, morphology studies and fluorescence lifetime imaging suggests that the spontaneous self-enhancement of the PCE and self-attenuation of the hysteresis is accompanied by the homogenization of the perovskite layer, improvements of charge extraction and reduced recombination. This understanding and kinetic data presented might can be adopted by researchers to facilitate stabilization of the initial performance of the PSC. The discussed effects are also important from the perspective of establishing reliable practices for the evaluation of the performance of PSCs basing on both *J-V* and quasi-steady-state measurements.

SUPPORTING INFORMATION

Experimental details; Tabulated photovoltaic parameters; detailed photovoltaic parameters evolution; TRPL curves and corresponding fitting parameters.

ACKNOWLEDGMENTS

SEM and XRD data presented in this manuscript were collected using the facilities at Monash Centre for Electron Microscopy and Monash X-ray platform. This work was financially supported by the National Natural Science Foundation of China (52002302, 22075221, 91963209), the Natural Science Foundation of Hubei Province (2020CFB172), and the National Key Research and Development Plan (SQ2019YFE010779). UB is grateful to the Australian Research Council (ARC) Centre of Excellence in Exciton Science (CE170100026) and the Australian Centre for Advanced Photovoltaics (ACAP) for the financial support. ANS gratefully acknowledges the financial support from ARC through the Future Fellowship (FT200100317).

REFERENCES

1. Wang, Y.; Duan, C.; Lv, P.; Ku, Z.; Lu, J.; Huang, F.; Cheng, Y.-B., Printing strategies for scaling-up perovskite solar cells. *Natl. Sci. Rev* **2021,** *8* (8), nwab075.
2. Min, H.; Lee, D. Y.; Kim, J.; Kim, G.; Lee, K. S.; Kim, J.; Paik, M. J.; Kim, Y. K.; Kim, K. S.; Kim, M. G.; Shin, T. J.; Il Seok, S., Perovskite solar cells with atomically coherent interlayers on SnO_2 electrodes. *Nature* **2021,** *598* (7881), 444-450.
3. Bu, T.; Li, J.; Li, H.; Tian, C.; Su, J.; Tong, G.; Ono, L. K.; Wang, C.; Lin, Z.; Chai, N.; Zhang, X.-L.; Chang, J.; Lu, J.; Zhong, J.; Huang, W.; Qi, Y.; Cheng, Y.-B.; Huang, F., Lead halide–templated crystallization of methylamine-free perovskite for efficient photovoltaic modules. *Science* **2021,** *372* (6548), 1327.
4. Dai, Z.; Yadavalli, S. K.; Chen, M.; Abbaspourtamijani, A.; Qi, Y.; Padture, N. P., Interfacial toughening with self-assembled monolayers enhances perovskite solar cell reliability. *Science* **2021,** *372* (6542), 618.
5. Jeong, J.; Kim, M.; Seo, J.; Lu, H.; Ahlawat, P.; Mishra, A.; Yang, Y.; Hope, M. A.; Eickemeyer, F. T.; Kim, M.; Yoon, Y. J.; Choi, I. W.; Darwich, B. P.; Choi, S. J.; Jo, Y.; Lee, J. H.; Walker, B.; Zakeeruddin, S. M.; Emsley, L.; Rothlisberger, U.; Hagfeldt, A.; Kim, D. S.; Grätzel, M.; Kim, J. Y., Pseudo-halide anion engineering for α-$FAPbI_3$ perovskite solar cells. *Nature* **2021,** *592* (7854), 381-385.
6. Wu, F.; Pathak, R.; Chen, K.; Wang, G.; Bahrami, B.; Zhang, W.-H.; Qiao, Q., Inverted current–voltage hysteresis in perovskite solar cells. *ACS Energy Lett.* **2018,** *3* (10), 2457-2460.
7. Liu, C.; Sun, J.; Tan, W. L.; Lu, J.; Gengenbach, T. R.; McNeill, C. R.; Ge, Z.; Cheng, Y.-B.; Bach, U., Alkali cation doping for improving the structural stability of 2D perovskite in 3D/2D PSCs. *Nano Lett.* **2020,** *20* (2), 1240-1251.
8. Kim, J. Y.; Lee, J.-W.; Jung, H. S.; Shin, H.; Park, N.-G., High-efficiency perovskite solar cells. *Chem. Rev.* **2020,** *120* (15), 7867-7918.
9. Guerrero, A.; Bou, A.; Matt, G.; Almora, O.; Heumüller, T.; Garcia-Belmonte, G.; Bisquert, J.; Hou, Y.; Brabec, C., Switching off hysteresis in perovskite solar cells by fine-tuning energy levels of extraction layers. *Adv. Energy Mater.* **2018,** *8* (21), 1703376.
10. Wang, C.; Xiao, C.; Yu, Y.; Zhao, D.; Awni, R. A.; Grice, C. R.; Ghimire, K.; Constantinou, I.; Liao, W.; Cimaroli, A. J.; Liu, P.; Chen, J.; Podraza, N. J.; Jiang, C.-S.; Al-Jassim, M. M.; Zhao, X.; Yan, Y., Understanding and eliminating hysteresis for highly

efficient planar perovskite solar cells. *Adv. Energy Mater.* **2017,** *7* (17), 1700414.
11. Moia, D.; Gelmetti, I.; Calado, P.; Fisher, W.; Stringer, M.; Game, O.; Hu, Y.; Docampo, P.; Lidzey, D.; Palomares, E.; Nelson, J.; Barnes, P. R. F., Ionic-to-electronic current amplification in hybrid perovskite solar cells: ionically gated transistor-interface circuit model explains hysteresis and impedance of mixed conducting devices. *Energy Environ. Sci.* **2019,** *12* (4), 1296-1308.
12. Walsh, A.; Stranks, S. D., Taking control of ion transport in halide perovskite solar cells. *ACS Energy Lett.* **2018,** *3* (8), 1983-1990.
13. Lu, J.; Jiang, L.; Li, W.; Li, F.; Pai, N. K.; Scully, A. D.; Tsai, C. M.; Bach, U.; Simonov, A. N.; Cheng, Y. B., Diammonium and monoammonium mixed-organic-cation perovskites for high performance solar cells with improved stability. *Adv. Energy Mater.* **2017**, *7*, 1700444.
14. Lu, J.; Lin, X.; Jiao, X.; Gengenbach, T.; Scully, A. D.; Jiang, L.; Tan, B.; Sun, J.; Li, B.; Pai, N.; Bach, U.; Simonov, A. N.; Cheng, Y.-B., Interfacial benzenethiol modification facilitates charge transfer and improves stability of cm-sized metal halide perovskite solar cells with up to 20% efficiency. *Energy Environ. Sci.* **2018,** *11* (7), 1880-1889.
15. Yoo, J. J.; Seo, G.; Chua, M. R.; Park, T. G.; Lu, Y.; Rotermund, F.; Kim, Y.-K.; Moon, C. S.; Jeon, N. J.; Correa-Baena, J.-P.; Bulović, V.; Shin, S. S.; Bawendi, M. G.; Seo, J., Efficient perovskite solar cells via improved carrier management. *Nature* **2021,** *590* (7847), 587-593.
16. Rong, Y.; Hu, Y.; Ravishankar, S.; Liu, H.; Hou, X.; Sheng, Y.; Mei, A.; Wang, Q.; Li, D.; Xu, M.; Bisquert, J.; Han, H., Tunable hysteresis effect for perovskite solar cells. *Energy Environ. Sci.* **2017,** *10* (11), 2383-2391.
17. Li, Z.; Xiao, C.; Yang, Y.; Harvey, S. P.; Kim, D. H.; Christians, J. A.; Yang, M.; Schulz, P.; Nanayakkara, S. U.; Jiang, C.-S.; Luther, J. M.; Berry, J. J.; Beard, M. C.; Al-Jassim, M. M.; Zhu, K., Extrinsic ion migration in perovskite solar cells. *Energy Environ. Sci.* **2017,** *10* (5), 1234-1242.
18. Roose, B.; Ummadisingu, A.; Correa-Baena, J.-P.; Saliba, M.; Hagfeldt, A.; Graetzel, M.; Steiner, U.; Abate, A., Spontaneous crystal coalescence enables highly efficient perovskite solar cells. *Nano Energy* **2017,** *39*, 24-29.
19. Habisreutinger, S. N.; Noel, N. K.; Snaith, H. J., Hysteresis index: a figure without merit for quantifying hysteresis in perovskite solar cells. *ACS Energy Lett.* **2018,** *3* (10), 2472-2476.
20. Jokar, E.; Chien, C.-H.; Fathi, A.; Rameez, M.; Chang, Y.-H.; Diau, E. W.-G., Slow surface passivation and crystal relaxation with additives to improve device performance and durability for tin-based perovskite solar cells. *Energy Environ. Sci.* **2018,** *11* (9), 2353-2362.
21. Jokar, E.; Chien, C.-H.; Tsai, C.-M.; Fathi, A.; Diau, E. W.-G., Robust tin-based perovskite solar cells with hybrid organic cations to attain efficiency approaching 10%. *Adv. Mater.* **2019,** *31* (2), 1804835.
22. Jokar, E.; Chuang, H.-S.; Kuan, C.-H.; Wu, H.-P.; Hou, C.-H.; Shyue, J.-J.; Wei-Guang Diau, E., Slow passivation and inverted hysteresis for hybrid Tin Perovskite Solar Cells Attaining 13.5% via Sequential Deposition. *J. Phys. Chem. Lett.* **2021,** *12* (41), 10106-10111.
23. Cho, Y.; Kim, H. D.; Zheng, J.; Bing, J.; Li, Y.; Zhang, M.; Green, M. A.; Wakamiya, A.; Huang, S.; Ohkita, H.; Ho-Baillie, A. W. Y., Elucidating mechanisms behind ambient storage-induced efficiency improvements in perovskite solar Cells. *ACS Energy Lett.* **2021,** *6* (3), 925-933.
24. Deng, Y.; Ni, Z.; Palmstrom, A. F.; Zhao, J.; Xu, S.; Van Brackle, C. H.; Xiao, X.; Zhu, K.; Huang, J., Reduced self-doping of perovskites induced by short annealing for efficient solar modules. *Joule* **2020,** *4* (9), 1949-1960.
25. Moghadamzadeh, S.; Hossain, I. M.; Jakoby, M.; Abdollahi Nejand, B.; Rueda-Delgado, D.; Schwenzer, J. A.; Gharibzadeh, S.; Abzieher, T.; Khan, M. R.; Haghighirad, A.

A.; Howard, I. A.; Richards, B. S.; Lemmer, U.; Paetzold, U. W., Spontaneous enhancement of the stable power conversion efficiency in perovskite solar cells. *J. Mater. Chem. A* **2020,** *8* (2), 670-682.
26. Fei, C.; Wang, H., Age-induced recrystallization in perovskite solar cells. *Org. Electron.* **2019,** *68*, 143-150.
27. Yamada, Y.; Endo, M.; Wakamiya, A.; Kanemitsu, Y., Spontaneous defect annihilation in $CH_3NH_3PbI_3$ thin films at room temperature revealed by time-resolved photoluminescence spectroscopy. *J. Phys. Chem. Lett.* **2015,** *6* (3), 482-486.
28. Bi, C.; Zheng, X.; Chen, B.; Wei, H.; Huang, J., Spontaneous passivation of hybrid perovskite by sodium ions from glass substrates: mysterious enhancement of device efficiency revealed. *ACS Energy Lett.* **2017,** *2* (6), 1400-1406.
29. Liu, Y.; Borodinov, N.; Lorenz, M.; Ahmadi, M.; Kalinin, S. V.; Ievlev, A. V.; Ovchinnikova, O. S., Hysteretic ion migration and remanent field in metal halide perovskites. *Adv. Sci.* **2020,** *7* (19), 2001176.
30. Correa-Baena, J.-P.; Anaya, M.; Lozano, G.; Tress, W.; Domanski, K.; Saliba, M.; Matsui, T.; Jacobsson, T. J.; Calvo, M. E.; Abate, A.; Grätzel, M.; Míguez, H.; Hagfeldt, A., Unbroken perovskite: interplay of morphology, electro-optical properties, and ionic movement. *Adv. Mater.* **2016,** *28* (25), 5031-5037.
31. Cho, A.-N.; Jang, I.-H.; Seo, J.-Y.; Park, N.-G., Dependence of hysteresis on the perovskite film thickness: inverse behavior between TiO_2 and PCBM in a normal planar structure. *J. Mater. Chem. A* **2018,** *6* (37), 18206-18215.
32. Tan, B.; Raga, S. R.; Chesman, A. S. R.; Fürer, S. O.; Zheng, F.; McMeekin, D. P.; Jiang, L.; Mao, W.; Lin, X.; Wen, X.; Lu, J.; Cheng, Y.-B.; Bach, U., LiTFSI-free spiro-OMeTAD-based perovskite solar cells with power conversion efficiencies exceeding 19%. *Adv. Energy Mater.* **2019,** *9* (32), 1901519.
33. Lu, J.; Scully, A. D.; Sun, J.; Tan, B.; Chesman, A. S. R.; Ruiz Raga, S.; Jiang, L.; Lin, X.; Pai, N.; Huang, W.; Cheng, Y.-B.; Bach, U.; Simonov, A. N., Multiple roles of cobalt pyrazol-pyridine complexes in high-performing perovskite solar cells. *J. Phys. Chem. Lett.* **2019,** *10* (16), 4675-4682.
34. Jung, E. D.; Harit, A. K.; Kim, D. H.; Jang, C. H.; Park, J. H.; Cho, S.; Song, M. H.; Woo, H. Y., Multiply charged conjugated plyelectrolytes as a multifunctional interlayer for efficient and scalable perovskite solar cells. *Adv. Mater.* **2020,** *32* (30), 2002333.
35. Jena, A. K.; Kulkarni, A.; Ikegami, M.; Miyasaka, T., Steady state performance, photo-induced performance degradation and their relation to transient hysteresis in perovskite solar cells. *J. Power Sources* **2016,** *309*, 1-10.
36. Hoke, E. T.; Slotcavage, D. J.; Dohner, E. R.; Bowring, A. R.; Karunadasa, H. I.; McGehee, M. D., Reversible photo-induced trap formation in mixed-halide hybrid perovskites for photovoltaics. *Chem. Sci.* **2015,** *6* (1), 613-617.
37. Dang, H. X.; Wang, K.; Ghasemi, M.; Tang, M.-C.; De Bastiani, M.; Aydin, E.; Dauzon, E.; Barrit, D.; Peng, J.; Smilgies, D.-M.; De Wolf, S.; Amassian, A., Multi-cation synergy suppresses phase segregation in mixed-halide perovskites. *Joule* **2019,** *3* (7), 1746-1764.
38. Gebhardt, J.; Rappe, A. M., Mix and match: organic and inorganic ions in the perovskite lattice. *Adv. Mater.* **2019,** *31* (47), 1802697.
39. Ferdani, D. W.; Pering, S. R.; Ghosh, D.; Kubiak, P.; Walker, A. B.; Lewis, S. E.; Johnson, A. L.; Baker, P. J.; Islam, M. S.; Cameron, P. J., Partial cation substitution reduces iodide ion transport in lead iodide perovskite solar cells. *Energy Environ. Sci.* **2019,** *12* (7), 2264-2272.
40. Liu, R.; Li, Z.; Chen, C.; Rao, Y.; Sun, X.; Wang, L.; Wang, X.; Zhou, Z.; Jiu, T.; Guo, X.; Frank Liu, S.; Pang, S., The possible side reaction in the annealing process of

perovskite layers. *ACS Appl. Mater. Interfaces* **2020,** *12* (31), 35043-35048.
41. Tong, G.; Son, D.-Y.; Ono, L. K.; Kang, H.-B.; He, S.; Qiu, L.; Zhang, H.; Liu, Y.; Hieulle, J.; Qi, Y., Removal of residual compositions by powder engineering for high efficiency formamidinium-based perovskite solar cells with operation lifetime over 2000 h. *Nano Energy* **2021,** *87*, 106152.
42. Rombach, F. M.; Haque, S. A.; Macdonald, T. J., Lessons learned from spiro-OMeTAD and PTAA in perovskite solar cells. *Energy Environ. Sci.* **2021**, *14*, 5161-5190.
43. Yin, C.; Lu, J.; Xu, Y.; Yun, Y.; Wang, K.; Li, J.; Jiang, L.; Sun, J.; Scully, A. D.; Huang, F.; Zhong, J.; Wang, J.; Cheng, Y.-B.; Qin, T.; Huang, W., Low-cost N,N′-Bicarbazole-Based Dopant-free hole-transporting materials for large-area perovskite solar cells. *Adv. Energy Mater.* **2018,** *8* (21), 1800538.
44. Lu, J.; Huang, F., Charge-carrying films for solar cells made quickly. *Nature* **2021**, *594*, 27-28.
45. Tress, W., Metal halide perovskites as mixed electronic–ionic conductors: challenges and opportunities: from hysteresis to memristivity. *J. Phys. Chem. Lett.* **2017,** *8*, 3106-3114.
46. Futscher, M. H.; Lee, J. M.; McGovern, L.; Muscarella, L. A.; Wang, T.; Haider, M. I.; Fakharuddin, A.; Schmidt-Mende, L.; Ehrler, B., Quantification of ion migration in $CH_3NH_3PbI_3$ perovskite solar cells by transient capacitance measurements. *Mater. Horizons* **2019,** *6* (7), 1497-1503
47. Haruyama, J.; Sodeyama, K.; Han, L.; Tateyama, Y., First-principles study of ion diffusion in perovskite solar cell sensitizers. *J. Am. Chem. Soc.* **2015,** *137* (32), 10048-10051.
48. Bryant, D.; Wheeler, S.; O'Regan, B. C.; Watson, T.; Barnes, P. R. F.; Worsley, D.; Durrant, J., Observable hysteresis at low temperature in "hysteresis free" organic–inorganic lead halide perovskite solar cells. *J. Phys. Chem. Lett.* **2015**, *6*, 3190-3194.
49. Pearson, A. J.; Eperon, G. E.; Hopkinson, P. E.; Habisreutinger, S. N.; Wang, J. T. W.; Snaith, H. J.; Greenham, N. C., Oxygen degradation in mesoporous $Al_2O_3/CH_3NH_3PbI_{3-x}Cl_x$ perovskite solar cells: kinetics and mechanisms. *Adv. Energy Mater.* **2016,** *6* (13), 1600014.
50. O'Regan, B. C.; Barnes, P. R.; Li, X.; Law, C.; Palomares, E.; Marin-Beloqui, J. M., Optoelectronic studies of methylammonium lead iodide perovskite solar cells with mesoporous TiO_2: separation of electronic and chemical charge storage, understanding two recombination lifetimes, and the evolution of band offsets during *J–V* hysteresis. *J. Am. Chem. Soc.* **2015,** *137* (15), 5087-5099.
51. Schubert, M. C.; Mundt, L. E.; Walter, D.; Fell, A.; Glunz, S. W., Spatially resolved performance analysis for perovskite solar cells. *Adv. Energy Mater.* **2020,** *10* (26), 1904001.
52. Quilettes, Dane W. De; Vorpahl Sarah, M.; Stranks Samuel, D.; Nagaoka, H.; Eperon Giles, E.; Ziffer Mark, E.; Snaith Henry, J.; Ginger David, S., Impact of microstructure on local carrier lifetime in perovskite solar cells. *Science* **2015,** *348* (6235), 683-686.
53. Tennyson, E. M.; Doherty, T. A. S.; Stranks, S. D., Heterogeneity at multiple length scales in halide perovskite semiconductors. *Nat. Rev. Mater.* **2019,** *4* (9), 573-587.
54. Ruggeri, E.; Anaya, M.; Gałkowski, K.; Delport, G.; Kosasih, F. U.; Abfalterer, A.; Mackowski, S.; Ducati, C.; Stranks, S. D., Controlling the growth kinetics and optoelectronic properties of 2D/3D lead–tin perovskite heterojunctions. *Adv. Mater.* **2019,** *31* (51), 1905247.
55. Yang, D.; Yang, R.; Wang, K.; Wu, C.; Zhu, X.; Feng, J.; Ren, X.; Fang, G.; Priya, S.; Liu, S., High efficiency planar-type perovskite solar cells with negligible hysteresis using EDTA-complexed SnO_2. *Nat. Comm.* **2018,** *9* (1), 3239.
56. Yan, W.; Li, Y.; Li, Y.; Ye, S.; Liu, Z.; Wang, S.; Bian, Z.; Huang, C., Stable high-performance hybrid perovskite solar cells with ultrathin polythiophene as hole-transporting layer. *Nano Res.* **2015,** *8* (8), 2474-2480.
57. Frost, J. M.; Walsh, A., What is moving in hybrid halide perovskite solar cells? *Acc. Chem. Res.* **2016,** *49* (3), 528-535.

58. Yang, J.-M.; Kim, S.-G.; Seo, J.-Y.; Cuhadar, C.; Son, D.-Y.; Lee, D.; Park, N.-G., 1D Hexagonal $HC(NH_2)_2PbI_3$ for multilevel resistive switching nonvolatile memory. *Adv. Electron. Mater.* **2018,** *4* (9), 1800190.
59. Pavlovetc, I. M.; Brennan, M. C.; Draguta, S.; Ruth, A.; Moot, T.; Christians, J. A.; Aleshire, K.; Harvey, S. P.; Toso, S.; Nanayakkara, S. U.; Messinger, J.; Luther, J. M.; Kuno, M., Suppressing cation migration in triple-cation lead halide perovskites. *ACS Energy Lett.* **2020,** *5* (9), 2802-2810.
60. Jiang, Y.; Remeika, M.; Hu, Z.; Juarez-Perez, E. J.; Qiu, L.; Liu, Z.; Kim, T.; Ono, L. K.; Son, D.-Y.; Hawash, Z.; Leyden, M. R.; Wu, Z.; Meng, L.; Hu, J.; Qi, Y., Negligible-Pb-waste and upscalable perovskite deposition technology for high-operational-stability perovskite solar modules. *Adv. Energy Mater.* **2019,** *9* (13), 1803047.
61. Saidaminov, M. I.; Kim, J.; Jain, A.; Quintero-Bermudez, R.; Tan, H.; Long, G.; Tan, F.; Johnston, A.; Zhao, Y.; Voznyy, O.; Sargent, E. H., Suppression of atomic vacancies via incorporation of isovalent small ions to increase the stability of halide perovskite solar cells in ambient air. *Nat. Energy* **2018,** *3* (8), 648-654.
62. Wu, J.; Liu, S.-C.; Li, Z.; Wang, S.; Xue, D.-J.; Lin, Y.; Hu, J.-S., Strain in perovskite solar cells: origins, impacts and regulation. *Natl. Sci. Rev.* **2021,** *8* (8), nwab047.